Chapter 5

Polarization dynamics in a CO_2 laser

I. Leyva, E. Allaria, R. Meucci

Abstract

We experimentally study the polarization dynamics of a quasi-isotropic CO_2 laser emitting on the fundamental and second order modes. We observe a complex dynamics in which spatial modes and polarization competition are involved. The observed dynamics is well reproduced by means of a model which provides a quantitative discrimination between the intrinsic asymmetry due to optical coherent coupling between sublevels, and the residual extrinsic anisotropies, due to cavity misalignments.

1 Introduction

Laser dynamics is commonly studied considering the electric field as a scalar variable, since in most systems the polarization state is imposed by anisotropies of the cavity. However, in perfectly cylindrical laser cavities without any elements to select a preferred polarization, the study of the dynamics includes the necessity of considering the vector nature of the electric field.

Several theoretical works have been devoted to the study of the polarization dynamics of the quasi-isotropic laser, showing the important role played by the material variables in the selection of the polarization state [1]. In particular, the degeneracy of the angular momentum states of the laser transition sublevels has been considered as the coupling source between different polarization states. Initial studies considered only stationary solutions [2, 3], but more recently dynamical models have been developed to explore the role of the anisotropy due to the laser medium [1, 4, 5, 6, 7]. These models show how the selection of circularly polarized or linearly polarized emission depends on the value of the total angular momentum of the lasing levels, and the relative magnitudes of the magnetic dipole and electric quadrupole relaxation rates of the sublevels. These studies predict a rich phenomenology even for the simplest transition, $J = 1 \rightarrow J = 0$. Later versions of these models include also linear and circular cavity anisotropies that we call extrinsic [8, 9], or different level structure [10].

Experiments carried out on gas lasers reveal that in some systems it is necessary to consider the dynamics of the matter variables to fully understand the polarization

features of an isotropic system [3, 11]. In other cases, the observations could be explained by a nonlinear coupling of the modes and residual cavity anisotropies [12, 13].

Up to now, most of the experiments in gas laser are performed in class A laser systems with simple level structure as He-Ne or He-Xe [6, 8], showing a good agreement for the steady state. In previous works, [14, 15], we have studied experimentally and theoretically the polarization behavior of a class B system (low pressure CO_2 laser), which has a higher order transition (J=19→ J=20) than those previously studied. We have shown that this complex structure makes the effective decay rate of the coherences to be closer to the decay rate of the population inversion rather than to the decay rate of the induced polarization [4, 15].

An intense research has been developed in the vectorial degrees of freedom of solid state lasers [16], due to their great interest in applications. Gas lasers however present some advantages when the interplay between spatio temporal dynamics and polarization dynamics has to be considered. In particular, they easily allow intracavity operation leading to tiny and controllable variations of extrinsic anisotropies. Some theoretical works consider competition effects via diffraction [17], or frequency anisotropies [13], but none of these studies consider the polarization competition driven by material variables when several transverse modes are present.

The work is structured as follow: in Sec. 2, we present the experimental arrangement used. In Sec. 3, we present the experimental results obtained for the steady and transient states. The model and numerical results are presented in Sec. 4. Further details of the model are given in the Appendix.

2 Experimental Setup

The experiment has been performed using an unpolarized Fabry-Perot cavity as shown in Fig. 1. The laser tube has a length of 35 cm and a transversal diameter of 2.5 cm. A total reflective flat mirror (M_1, reflectivity R_1=1) and an outcoupler mirror (M_2) with a reflectivity $R_2 = 0.914$ set the cavity length at L =75 cm. A piezo translator (Pzt) is used to select the P(20) laser emission line and to adjust the laser detuning. An intracavity diaphragm allow us to adjust the aperture of the cavity in order to allow laser action just for the first two transversal family modes of the only longitudinal mode which is active.

The active medium, a mixture of He (82%), N_2 (13.5%) and CO_2 (4.5%) at a pressure of 25 mbar, is pumped by a DC discharge fixed at 6.1 mA when the threshold current is 3 mA. Therefore, the pump strength is fixed at twice over the laser threshold during the experiments.

The polarization state of the laser emission has been analyzed by means of a wire grid polarizer (Pol), which has the property of reflecting one linear polarization of the incident radiation and transmitting the orthogonal one, with an extinction ratio of 1:180. The reflected and transmitted parts of the beam are directed to two HgCdTe fast detectors (D_1, D_2, 100 MHz bandwidth), whose sensitive areas (10^4 μm^2) are much smaller than the beam size. Both signals are recorded on a digital oscilloscope (Lecroy LT423L) with 500 MHz bandwidth. The transverse intensity

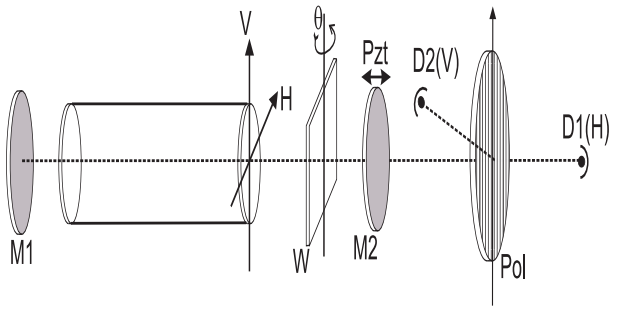

Figure 1: Experimental setup: M_1: total reflecting flat mirror, W: additional intracavity window, M_2: outcoupler mirror, V: Vertical axis of the cavity, H: Horizontal axis of the cavity, Pzt: piezo electro translator, Pol: wire grid polarizer, D_1(V): fast detector for the horizontal component, D_2(H): fast detector for the vertical component. A piroelectric camera sustitues D_1(H) for the spatial transerve intensity profile measurements.

profile is been recorded by means of an infrared pyroelectric videocamera (Spiricon Pyrocam III, model PY-III-C-A) connected to a computer.

We observe that for any configuration, the laser has two possible linear polarization directions which are orthogonal as far as we can measure [15]. In Fig. 1 these cavity eigendirections are called H and V respectively.

As we are also interested in the transient dynamics, an intracavity chopper is eventually used to induce a switch-on event at a repetition rate of 200 Hz.

3 Experimental Results

Our aim is the study of the polarization dynamics in the steady state and the switch-on transient of a CO_2 laser, and the interplay between the polarization competition and the spatial dynamics. For these purpouses, we perform two experiments. First, we observe the polarization dynamics when just the fundamental mode TEM_{00} is allowed to emit. In this configuration without spatial degrees of freedom, we can observe how the polarization dynamics is affected by losses and detuning anisotropies. In a second experiment, the laser diaphagm is open such as both the fundamental and the second order modes TEM_{01} and TEM_{10} are allowed to emit. In this configuration we observe how the polarization inestabilities coexits with the spatial competition.

3.1 Dynamics of the fundamental mode

In the first experiment, the laser aperture is adjusted in such a way that only the TEM_{00} mode emit. In the stationary regime, we observe that the laser has two possible linear polarization directions which are orthogonal as far as we can measure. In Fig. 1 these cavity eigendirections are called H and V respectively.

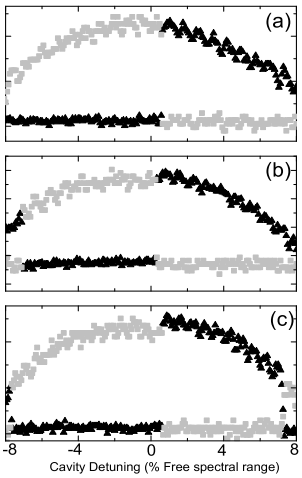

Figure 2: Experimental intensity of both polarization components along a free spectral range (Black triangles vertical polarization direction, gray squares horizontal polarization direction) (a) quasi isotropic condition $\theta = 0$ (b) $\theta = 6^o$ (c) $\theta = 9^o$. It is to be noted that a Pzt adjustement is required to recover the resonant condition for each θ.

As we want to study the effect of the cavity anisotropies in the dynamics, the introduce an intracavity window W that can rotate by an angle θ around the axis V. When $\theta = 0$, the polarization direction is determined by the detuning of the cavity, as usual [3, 8, 19]. This is illustrated in Fig.2(a), where we plot the laser intensity along both eigendirections when the detuning is varied around the line center. A residual hysteresis around the transition is masked by the limited resolution of Pzt. At the transition point near the line center there is not a preferred polarization direction and the laser flips spontaneously from one to other due to noise, as shown in Fig. 3.

We center our study of the polarization behavior in this bistable region. In particular, we analyze the switch-on transient state, in which the total intensity presents relaxation oscillations. In our system the pump strength, fixed at twice over the laser threshold, imposes a relaxation frequency of 55 KHz.

When the two polarized components are separated, they show oscillations in relative antiphase, which do not appear on the total intensity (Fig.4). The amplitude of these oscillations depends on the angle between the polarizer axes with respect to H-V, reaching a maximum when the analysis is performed at 45^o.

In Fig.4(a) we report an example of these polarization oscillations, when the cavity is tuned at the center of the line. The total laser output intensity (thick solid line) is displayed together with its two orthogonally polarized components analyzed at 45^o (thin solid and dashed lines).

These oscillations are always damped until they disappear, with a damping rate

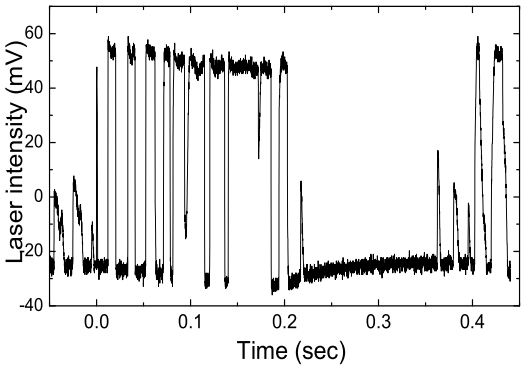

Figure 3: Intensity of vertical polarization component when the cavity detuning is chosen at the transition point near the resonance.

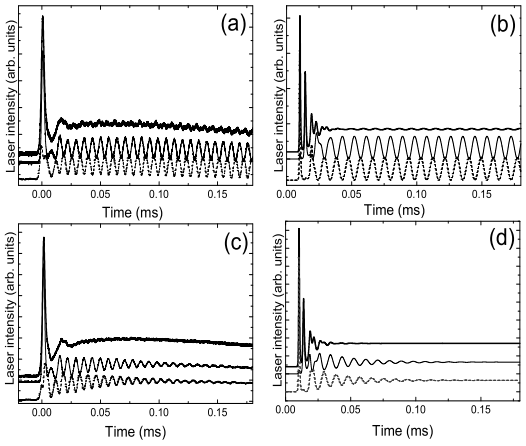

Figure 4: Experimental time intensity profiles of the total intensity (solid line) and both polarization components (thin solid and dotted lines) for $\theta = 0$ and slightly different detuning condition : (a) resonance, (c) out of resonance. Numerical generated intensity profiles for θ=0, $\alpha = \beta = 0.01$ and : (b) $\delta = 0$, (d) $\delta = 0.05$. The curves have been vertically shifted for a better observation.

depending on the cavity detuning. Precisely the oscillations are more persistent the closer is the detuning to the bistable region. This fact points to the competitive origin of the oscillations. In Fig.4 (c) we show an example of the transient dynamics when the cavity detuning is slightly moved from resonance. It is worth to note that the system is so sensitive to noise that the duration of the oscillations suffers slight variations, without apparent changes in the conditions.

Successively, we studied the response of the system to small linear anisotropies driven by the tilt angle θ of the intracavity window W around the vertical axis.

Several parameters of the system are simultaneously affected by this action. As a consequence of the common increasing of the optical path for both polarization eigendirections, the line center moves with respect to the isotropic condition $\theta = 0$. In order to keep the bistable condition, the cavity length is varied to recover the resonance.

In Fig.2((b) and (c)) we plot the intensity of both polarization components for different θ values, showing that the gain profile is not significantly distorted with respect to the isotropic condition $\theta = 0$ (Fig.2(a)). The detuning anisotropies (i.e. the slight frequency difference between the two eigenpolarization modes due to the tilted window and other residual cavity anisotropies) are measured to be smaller than 5% of the total change.

The other effect of the tilt angle θ is to increase the total cavity losses. Since the gain profiles for the two polarization directions do not change due to the tilt angle θ (Fig. 2), we can assume that the induced loss anisotropies remain a small effect ($\simeq 1\%$) compared to the total loss change. The effect of the losses anisotropy can be observed in the residual modulation in the total intensity (Figs.4 (a),(c)).

The dynamical effect observed when θ is increased is the growing of the frequency of the polarization oscillations. Measurements made near the resonance condition show that the frequency rises as the tilt angle increased(Fig.5 (a)). It can be seen that a tilt angle of 12^o is enough to rise the frequency from 100 KHz to 400 KHz.

Furthermore, we have also experimentally tested that, in contrast with the relaxation oscillation, the frequency of the polarization oscillation does not depend on the discharge current when its value is increased from I_{thre} up to aproximatelly $3\mathrm{I}_{thre}$.

3.2 Dynamics of the second order modes

Once we know the system behaviour in the fundamental mode, we increase the laser aperture to allow emission of the second order modes TEM_{01} and TEM_{10}. Our next goal is to observe simultaneous spatial and polarization dynamics in the system. In order to simplify the analisys, in this case we do not use the intracavity window W, to mantain the cilindrical symmetry, apart from the unavoidable residual astigmatism. As in the previous case, the system is characterized first in the stationary regime, then the transitory switch-on regime is studied [18].

In the stationary regime, measurements performed by means of the pyroelectric camera reveal that the spatial profile of the intensity has a doughnut-like shape, as usual. If the polarization state is analyzed along the H-V axes, we find two polar-

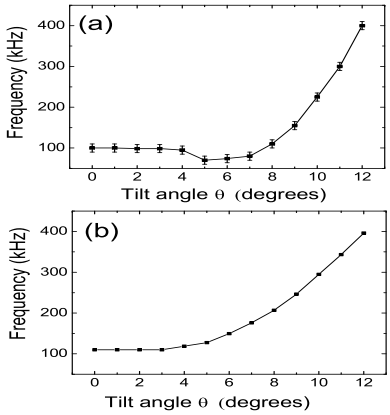

Figure 5: Polarization oscillation frequency as a funtion of the tilt angle: (a) experimental, (b) numerical ($\delta = 0$, α=0.01 β=0.01)

ization configurations for this annular pattern, depending on the detuning value, as it is well known [3, 8, 19]. Thus, when the cavity detuning is set around the center of the gain line, the annular pattern consists of a TEM_{10} mode polarized along the eigendirection H and a TEM_{01} mode polarized along the eigendirection V (Fig. 6 (a)). In the following, we will call this configuration *splitted*. The total intensity presents a periodic modulation with at a frequency of 2.2 MHz, as shown in (Fig. 6 (b)). This pattern is stable in a quite narrow detuning range around the resonance condition $\delta = 0$. It is to note that we have never observed the opposite configuration, i.e., a TEM_{01} mode polarized along the eigendirection V and a TEM_{10} mode polarized along the eigendirection H.

When the cavity is set far from atomic resonance, the pattern change to a homogeneously polarized ring along the eigendirection V (Fig. 6 (c)). The total intensity presents a periodic modulation at 2.6 MHz (Fig. 6 (d)), having a much larger statility range than the splitted one. From now on, we call this the *homogeneous* configuration.

We never observe spontaneous polarization flips, in contrast with in the case of the TEM_{00} mode emission, in which spontaneous flips between both possible polarization states (H-V) where found near resonance as stated in Sec. 3.1.

In both splitted and homogeneous configurations, the frequency of the described oscillation of the total intensity is far from the beating of two consecutive transverse order modes, which in our case is 72 MHz. [20]. Therefore, this periodic undamped oscillation of the total laser output intensity corresponds to the mode beating of the two second order modes, after their frequency degeneration is broken by cavity astigmatism [21, 22].

Once the steady state has been characterized, we introduce the intracavity chopper in order to induce a switch-on transient. The observed transient behavior corresponds to the two configurations reported in Fig. 6, found around resonance

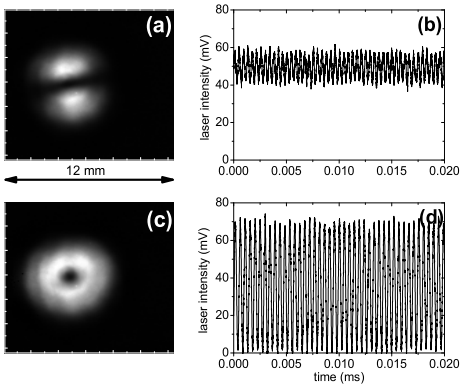

Figure 6: Experimental steady configuration. (a,b) Around resonance: (a) Average spatial profile polarized along the H eigendirection, (b) Laser total intensity time dependence for (a). (c,d) Far from resonance: (c) Average spatial profile polarized along the H eigendirection, (d) Laser total intensity time dependence for (c).

(splitted) and far from resonance (homogeneous), respectively.

In the splitted case (Fig. 7), the polarized intensity shows clearly the appearance of two consecutive transients, about 0.5 ms apart, corresponding to the rising of the fundamental and secondary modes respectively (Fig. 7 (a)). In both transients, we find the same characteristic polarization competition oscillations already observed in the fundamental case. These oscillations have the same frequency around 100 KHz for both the onset of the fundamental and the second order modes, which allows us to discard a possible origin in spatial competition. In Fig. 7 (b) we detail the transient corresponding to the birth of the second order modes, to show how the polarization oscillation at 100 KHz and the beating modulation at 2.2 MHz are simultaneously present.

After this second transient, the polarization competition dumps to disappear and only the beating oscillation persists, as observed in steady state measurements. Unfortunately, the temporal resolution of the pyrocamera is not fast enough as to follow the evolution of the whole pattern during this transient.

In the second case in which the observation is performed far from resonance (Fig. 8), we find again that same polarization oscillation at the onset of the first and second order modes (Fig. 8(a)). The change in the detuning does not affect to the frequency of the polarization competition, whereas the beating whose frequency changes from 2.2 MHz to 2.6 MHz, as shown above. In Fig. 8 (b) we show how during the transient of the second order modes the geometrical competition appears as a stronger modulation to the polarization oscillation than in the resonant case Fig. 7 (b).

In conclusion, our experiments seem to confirm the presence of a simultaneous spatial and polarization competition during the transitory regime of a transverse

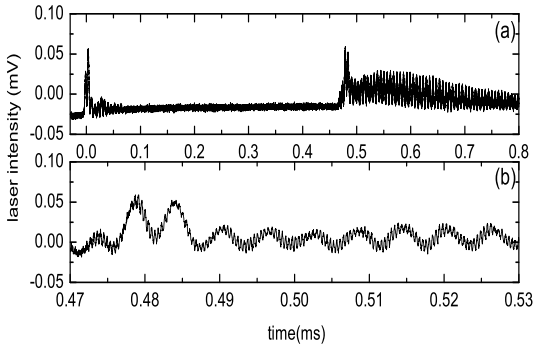

Figure 7: (a) Intensity time profile of a polarized component during the transient splited configuration. (b) Detail of (a) showing the transient of the secondary order modes.

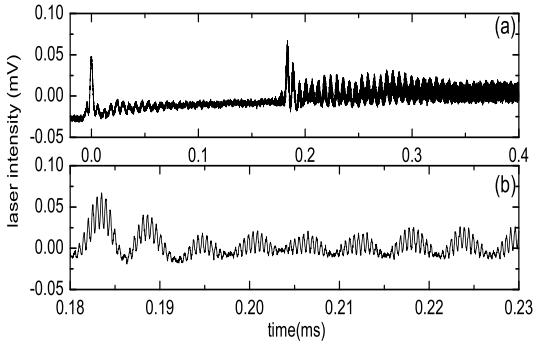

Figure 8: (a) Intensity time profile of a polarized component during the transient homogeneous configuration. (b) Detail of (a) showing the transient of the secondary order modes.

multimode emission.

4 Model and numerical results

Our theoretical approach is based on the theory of the isotropic laser developed in Ref. [4] where the optical coherences between upper levels are considered. This theory was developed for the simplest case (J=1 → J=0), while the transition involved in our system is much more complicated (J=19 → J=20). However, this theory has been showed to predict also the behavior of lasers with a different level structure, as shown in Ref. [8, 11], where an effective value of the coherence decay rate was deduced.

Only first order coherences ($\Delta m = \pm 1$) will be considered. Therefore, independently of the number of sublevels, there are only two kinds of possible transitions, which generate a split of the population in two ensembles, in such a way that an anisotropy is induced in the active medium [6]. Furthermore we introduce an extrinsic linear anisotropy as done in Ref.[8], to reproduce the effect of the intracavity window or any other astigmatism source.

The field will be decomposed in a circularly polarized basis. Just losses and linear detuning anisotropies along the principal axes of the system will be included, but not circular asymmetries since our system does not show signs of dichroism. It reads [1]:

$$\begin{aligned}
\dot{E_R} &= \kappa(P_R - E_R) + i\delta E_R - (\alpha + i\beta)E_L + ia(\mathbf{\Delta} - 4\rho^2)E_R \\
\dot{E_L} &= \kappa(P_L - E_L) + i\delta E_L - (\alpha + i\beta)E_R + ia(\mathbf{\Delta} - 4\rho^2)E_L \\
\dot{P_R} &= -\gamma_\perp[P_R - D_R E_R - E_L C], \\
\dot{P_L} &= -\gamma_\perp[P_L - D_L E_L - E_R C^*], \\
\dot{C} &= -\gamma_c C - \frac{\gamma_\parallel}{4}(E_L^* P_R + E_R P_L^*) \\
\dot{D_R} &= -\gamma_\parallel[D_R - r + \frac{1}{2}(E_R P_R^* + E_R^* P_R) + \frac{1}{4}(E_L P_L^* + E_L^* P_L)], \\
\dot{D_L} &= -\gamma_\parallel[D_L - r + \frac{1}{2}(E_L P_L^* + E_L^* P_L) + \frac{1}{4}(E_R P_R^* + E_R^* P_R)]
\end{aligned} \tag{1}$$

where $E_R(\vec{r},t), E_L(\vec{r},t)$ are the slowly varying electric fields. $P_R(\vec{r},t), P_L(\vec{r},t)$ stand for the matter polarization fields, $D_R(\vec{r},t)$ and $D_L(\vec{r},t)$ are the respective population inversions and $C(\vec{r},t)$ is the coherence field. $r(t)$ is the rescaled pump. The transverse coordinates are rescaled as $(\nu,\eta) = (x,y)/w_0$, being $w_0^2 = \lambda\sqrt{L(r_2 - L)/\pi}$ the minimum beam waist. The factor $\rho^2 = \nu^2 + \eta^2$ is the transverse distance to the mirror center. Therefore, $\mathbf{\Delta} = \partial_\nu^2 + \partial_\eta^2$ is the transverse Laplacian and a=$\lambda c/(4\pi w_0^2)$ is the diffraction coefficient.

The parameter r(t), fixed to a value of 2.0, stands for the pump strength normalized to its threshold value. The field $C(\vec{r},t)$ represents the coherence between the upper sublevels. We recall that, in a density matrix treatment, the polarization corresponds to off diagonal matrix elements between upper and lower level of the radiative transition, whereas C is proportional to the off diagonal matrix elements coupling different angular momentum states of the upper level [11]. The parameter δ represents the detuning between the cavity and the atomic transition frequencies.

The parameters $\alpha = (\kappa_V - \kappa_H)/2$ and $\beta = (\delta_H - \delta_V)/2$ represent respectively the linear anisotropies in the losses and detuning with respect to the cavity H-V axes, where κ_V, κ_H, are the losses in the horizontal and vertical axis, and δ_V, δ_H are the corresponding detunings.

In our low pressure CO_2 laser, the polarization decay is $\gamma_\perp = 4.4 \cdot 10^8$ s^{-1} and the inversion decay rate as $\gamma_\parallel = 1.95 \cdot 10^5 \text{s}^{-1}$ [14].

The parameter δ represents the detuning between the cavity and the atomic transition frequencies. We denote by ω_a the central frequency of the only active atomic transition, which is the P(20) line. We denote as ω the field frequency without taking into account the transverse contribution to the eigenfrequency. Thus $\delta = (\omega_a - \omega)/\gamma_\perp$ is the rescaled cavity detuning of the modes from the central atomic transition frequency, apart from the transverse frequency shift, which will be considered later when needed.

The parameters $\alpha = (\kappa_V - \kappa_H)/2$ and $\beta = (\delta_H - \delta_V)/2$ stand for the linear anisotropies in the losses and detuning with respect to the cavity H-V axes, respectively. Here κ_V, κ_H, are the losses in the H an V axis respectively, and δ_V, δ_H are the corresponding detunings.

4.1 Numerical results for the dynamics of the fundamental mode

When just the fundamental mode is included in the dynamics, the mirrors effect can be neglected [20], or equivalently it can be supposed than the fields E, P, D and C are spatially homogeneous. Therefore the Eqs. 1 become a set of ordinary differential equations, already described in Ref. [1].

All the parameter have been defined above but γ_c, representing the coherence decay rate, whose value should be chosen between $\gamma_\perp$ and $\gamma_\parallel$ [1]. However, this parameter cannot be directly measured, and it will be used as control parameter in order to fit the theory to the experimental results [8]. We find that the optimal value is $\gamma_c \simeq \gamma_\parallel$ in all cases, which is also consistent with the observation that just linearly polarized states are found in the experiment. Indeed, a higher value of γ_c would give rise to a periodic modulation of the total intensity which has never been observed in our experiments [1]. Both the polarization and coherences decay rates are related to molecular collisions, but how these affect the induced polarization and the inner sublevel coherence can be different. A physical reason for the small effective value for γ_c in the CO_2 laser can be found in the complexity of the upper and lower sublevel structures. The elastic collisional processes which interrupt the phase of the emission (contributing to $\gamma_\perp$) produce a minor effect on optical coherences as compared with that induced in the simplest case (J=1 $\rightarrow$ 0). In this last situation only a lower sublevel exists and collisions easily induce changes on the two population ensembles.

Once we have fixed the value $\gamma_c \simeq \gamma_\parallel$ to quantify the effect of the intrinsic anisotropy, we proceed to quantify the effect of the extrinsic anisotropy driven in the experiment by the tilted window W. As said in Sec. 3.1, from the experimental observations we know that the most important effect of the window tilting is the increase of the total losses, while loss and detuning anisotropies, as well as pump

changes, represent a minor effect on the polarization oscillation. For the relevant parameter κ we assume the following angular dependence [23]:

$$\kappa(\theta) = \kappa_o(1 + a_k \sin^4(\theta)) \tag{2}$$

where $\kappa_o = -\frac{c}{4L} log(R) = 4.1 \cdot 10^6$ s^{-1} are the pump strength and total losses when the tilt angle $\theta = 0$. Here c is the speed of light, $L = 0.75$ m the cavity length and $R = \sqrt{R_1 R_2} = 0.956$ the mirrors reflectivity. The parameter a_κ consider the effect of the multiple reflection on the intracavity window W over the total losses. It value have been obtained by fitting the experimental data on the angular dependence of the polarization frequency presented in Fig. 6 (a). The resulting value is $a_\kappa = 4500$.

In Fig. 4 (b) and (d) the numerically generated intensity profiles are compared with their experimental counterparts reported in Fig 4 (a) and (c), respectively. It can be observed that the intensity profiles show antiphase oscillations for both polarization components, while the total intensity remains unmodulated.

When δ=0, the polarization oscillations remain undamped for any degree of anisotropy. For $\delta \neq 0$, the oscillations are still undamped only in perfect cavity symmetry conditions $\alpha = \beta = 0$. In Fig.4 (d) it can be seen that for $\delta = 0.05$, a detuning or losses anisotropy of 0.5 % is sufficient to damp the oscillation in a few hundred microseconds as observed in the experiment. In the experimental system unavoidable residual anisotropies break the cylindrical symmetry, and therefore the polarization oscillations are always damped.

Choosing the resonant condition $\delta = 0$, we observe that the frequency of the oscillations presents the same dependence on the total losses found in the experiment described in Sec. 3.1. In Fig. 5 we compare the experimental and numerical angular dependences of the polarization oscillation frequency (Fig. 5 (a),(b)), showing a good agreement.

4.2 Numerical results for the dynamics of the second order modes

When the spatial degrees of freedom are included, the full spatio-temporal integration of Eqs. 1 would be prohibitive, taking into account the presence of several fields and the stiffness of the problem. However, since the pump value is not far from threshold, we can simplify the above system in a set of ordinary differential equations, using the mode expansion technique for all the fields and the population inversion [24, 25, 26]. From the experimental results we know that just the TEM_{00}, TEM_{01} and TEM_{10} take part in the dynamics, and therefore the general expression of the variables as linear combination of these three modes is:

$$\begin{aligned} E_{R(L)}(\nu,\eta,\tau) &= \sum_{j=0}^{2} A_j(\nu,\eta) e_{j,R(L)}(\tau) \\ P_{R(L)}(\nu,\eta,\tau) &= \sum_{j=0}^{2} A_j(\nu,\eta) p_{j,R(L)}(\tau) \\ D_{R(L)}(\nu,\eta,\tau) &= \sum_{k=0}^{5} B_k(\eta,\nu) d_{k,R(L)}(\tau) \end{aligned} \tag{3}$$

$$C(\nu,\eta,\tau) = \sum_{k=0}^{5} B_k(\eta,\nu)c_k(\tau)$$

where $e_{j,R(L)}(\tau), p_{j,R(L)}(\tau)$, $d_{k,R(L)}(\tau)$ and $c_k(\tau)$ are the temporal evolution profiles of the variables. The mode spatial functions $A_j(\nu,\eta), j = 0,1,2$ are the standard Gauss-Hermite modes TEM_{00}, TEM_{01} and TEM_{10} respectively:

$$\begin{aligned} A_0(\nu,\eta) &= \sqrt{\frac{2}{\pi}} exp(-\rho^2) \\ A_1(\nu,\eta) &= 2\eta A_0(\nu,\eta) \\ A_2(\nu,\eta) &= 2\nu A_0(\nu,\eta) \end{aligned} \tag{4}$$

Likewise, the population inversions and coherence field have been expanded in the orthonormal basis [26]:

$$\begin{aligned} B_0(\nu,\eta) &= \sqrt{\pi} A_0^2(\nu,\eta)\ , \\ B_1(\nu,\eta) &= \sqrt{\pi}(A_1^2(\nu,\eta) - A_2^2(\nu,\eta))\ , \\ B_2(\nu,\eta) &= \sqrt{\pi}(A_1^2(\nu,\eta) + A_2^2(\nu,\eta) - A_0^2(\nu,\eta)) \\ B_3(\nu,\eta) &= \sqrt{2\pi} A_0(\nu,\eta)A_1(\nu,\eta)\ , \\ B_4(\nu,\eta) &= \sqrt{2\pi} A_0(\nu,\eta)A_2(\nu,\eta)\ , \\ B_5(\nu,\eta) &= \sqrt{4\pi} A_1(\nu,\eta)A_2(\nu,\eta)\ . \end{aligned} \tag{5}$$

Each transverse mode has a slightly different frequency, and therefore the detuning δ has also to be splitted to take into account these differences. We denote by $\Omega_{00}, \Omega_{01}, \Omega_{10}$ each mode frequency shift due to the curved mirrors, rescaled to $\gamma_\perp$, respectively. In the ideal case, the TEM_{01} and TEM_{10} modes are frequency degenerated $\Omega_{01} = \Omega_{10} = 2\Omega_{00}$, but the breaking of this degeneracy is usual in the experiment [12, 13, 21]. In this case, the second order modes symmetrically split from their original frequency, $2\Omega_{00}$. In order to take into account this symmetry breaking, an additional parameter $d\omega$ becomes necessary [27]. Finally, the frequencies of each transverse mode are:

$$\begin{aligned} \Delta_0 &= \delta + \Omega_{00} \\ \Delta_1 &= \delta + 2\Omega_{00}(1 + d\omega) \\ \Delta_2 &= \delta + 2\Omega_{00}(1 - d\omega) \end{aligned} \tag{6}$$

Notice that in this way, each second order mode suffers two deviations in its frequency, with respect to the ideal case. First, a frequency difference which apart each other the TEM_{01} and TEM_{10} modes with the same polarization. This difference is represented by the parameter $d\omega$ [13, 21]. In addition, we have considered that the cavity is astigmatic respect to the polarization, and therefore each vertically polarized mode is separated in frequency from its horizontal homologous by a frequency anisotropy represented in the model by β. We have choose to separate both effects to give account of their respective importance in the dynamics.

The modelization of the transient dynamics includes the effect of the relatively low speed of the intracavity chopper in the spatial distribution of the gain. In order

to reproduce it, the fundamental mode gain ($r_0(t)$) is going to be considered to have a faster grow than the secondary mode gain ($r_2(t)$), where:

$$\begin{aligned} r_0(t) &= r(1 - e^{(t_0-t)/a}) \\ r_2(t) &= r(1 - e^{(t_2-t)/a}) \end{aligned} \tag{7}$$

being r=2.0 the final gain value. Since in the model the lasing threshold value for the fundamental mode is r_{th}=1.0, this means a value approximately twice higher than the fundamental mode threshold, as in the experiment. The other parameters, $t_0 = 200\gamma_\perp$, $t_2 = 45000\gamma_\perp$ and a=$150\gamma_\perp$ are chosen to fit the experimental rising rates of the modes.

Inserting all these expansions in the Eqs. (1), we obtain a set of equations describing the interaction among the 6 modes (3 for each polarization) present in the dynamics. The complete set of equations, in the more general form, can be found in the Appendix.

By means of this model we reproduce most of the experimental observations reported in Sec. 3. In order to reduce the large numbers of parameters involved in the simulations, we consider the cavity losses as perfectly isotropic, taking $\alpha = 0$ in all cases.

Numerical calculations of the steady state show a dependence on the detuning similar to that observed in the experiment. The behavior of the total intensity shows a periodic modulation whose frequency depends only on the value of $d\omega$, the detuning difference anisotropy between the secondary order modes. Therefore, we can associate this stable modulation to the degeneration frequency or the secondary order modes. Unfortunately, we have not experimental control of this parameter, in contrast with the case studied in the Ref. [21]. Accordingly to Tamm., a progressive decrease of $d\omega$, approaching to resonance condition, yields a chaotic fluctuation of the intensity which has been never observed in the experiment. This give us a effective measure of the value of the symmetry breaking in our experiment. In order to obtain the same frequency (around 2 MHz.) observed in the experiment, we set this parameter to $d\omega = 0.007$, a very small percentage compatible with spontaneous symmetry breaking. As it was observed in the experiment, the modulation percentage is smaller for small detuning value ($\delta = 0.1$, Fig. 9(c)) than for large detuning values ($\delta = 0.7$, Fig. 9(d))which indicates that the symmetry breaking slightly increases when δ increases.

Once the steady state has been characterized and contrasted with the experiment, the reproduction of the transient dynamics is explored. In this case, the evolution of the total intensity reproduces the two consecutive transients corresponding to the onset of the fundamental and secondary order modes, respectively. When the intensity of each polarized component is calculated, we observe in transients a out of phase oscillations at $\simeq$ 100 KHz.

The similarity between numerical results and experiments can be seen from Fig. 10 (a), where we plot the temporal evolution for a linearly polarized component, in a case of relatively small detuning (δ=0.1), to be compared to its experimental counterpart in Fig. 7 (a). Here both transients are presents, and a final state slightly modulated can be observed. In Fig. 10 (b) we detail the dynamics around

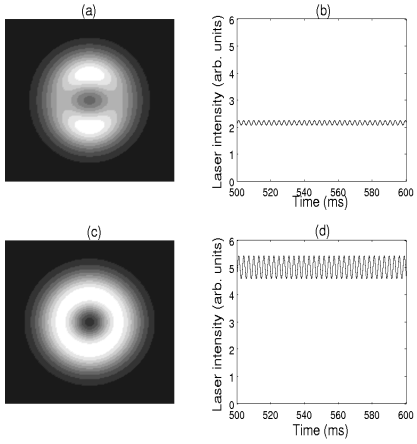

Figure 9: Numeric steady configuration. Near resonance for $\delta = 0.1$, : (a) Average spatial profile polarized along the H eigendirection, , (b) Laser total intensity time dependence for (a). Far from resonance for $\delta = 0.7$: (b) Spatial profile polarized along the H eigendirection, (d) Laser total intensity time dependence for (c)static

the secondary transient. In Fig. 11 we plot the temporal evolution in the case of large detuning (δ=0.7), to be compared to its experimental counterpart shown in Fig. 8. In this case, it can be clearly observed in Fig. 10 (b) how the polarization oscillation at 100 KHz is modulated by the faster beating oscillation at 2MHz.

The importance of the coherence term C to reproduce the observed dynamics can be appreciated in Fig. 12. Here we plot the vertical polarized component for a case analogous to that reported in Fig. 8 ($\delta = 0.7, d\omega = 0.007, d\delta = 0.025$), but in which the coherence term is set $C = 0$. It can be appreciated that the out-of phase polarization oscillations disappear, confirming that this dynamics observed in the experiment depends on the interaction through the material variables.

5 Conclusions

In conclusion, we have reported an experimental and theoretical study of the spatiotemporal polarization dynamics of a quasi-isotropic CO_2 laser. The simultaneous polarization and spatial competition dynamics observed can be reproduced by means of a model including both vectorial and spatial degrees of freedom. The results point out the important role played by optical coherence effects in spatio temporal laser dynamics.

Acknowledgments

The authors are grateful to F.T. Arecchi for the fruitful discussions. I. Leyva and E. Allaria wish to acknowledge the support of the European Project HPRN-CT-2000-00158.

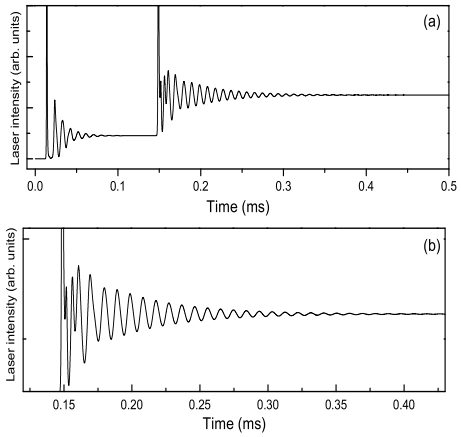

Figure 10: (a)Numerical generated laser intensity evolution for a polarized component, with $\delta = 0.1, \Delta\delta = 0.025, \Delta\omega = 0.007$, (b) detail of (a) around the polarization oscillation in the transient of the second order modes.

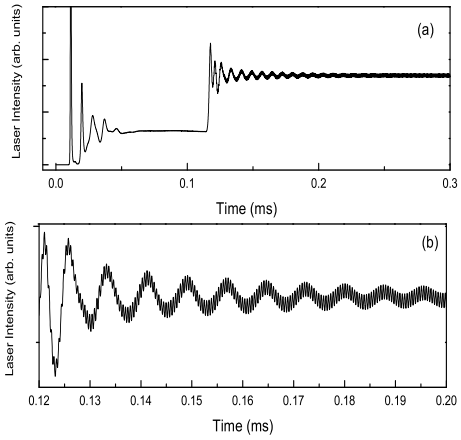

Figure 11: (a)Numerical generated laser intensity evolution for a polarized component, with $\delta = 0.7, \Delta\delta = 0.025, \Delta\omega = 0.007$. (b) Detail of (a) around the polarization oscillation in the transient of the second order modes

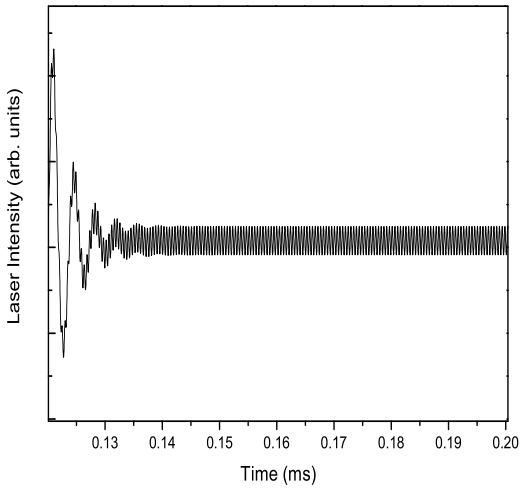

Figure 12: Detail of the numerical generated laser intensity evolution for a polarized component, with δ=0.7, d δ=0.025, $\Delta\omega$ =0.007 and $C = 0$

*

A Appendix

In this Appendix we explicitly shown the equations for the modal amplitudes [26]: $\dot{e}_{j,R(L)} = \kappa(b_{j,R(L)} - e_{j,R(L)}) + i\Delta_j e_{j,R(L)} - (\alpha + i\beta)e_{j,R(L)}$

$$\dot{p}_{0,R(L)} = -p_{0,R(L)} + \tfrac{1}{\sqrt{\pi}}\left[m(0,0)_{R(L)} + \tfrac{1}{\sqrt{2}}\left(m(1,3)_{R(L)} + m(2,4)_{R(L)}\right)\right]$$

$$\dot{p}_{1,R(L)} = -p_{1,R(L)} + \tfrac{1}{\sqrt{\pi}}[\tfrac{1}{\sqrt{2}}m(0,3)_{R(L)} + \tfrac{1}{2}(m(0,1)_{R(L)} + m(1,1)_{R(L)} + m(1,2)_{R(L)} + m(2,5)_{R(L)})]$$

$$\dot{p}_{2,R(L)} = -p_{2,R(L)} + \tfrac{1}{\sqrt{\pi}}[\tfrac{1}{\sqrt{2}}m(0,4)_{R(L)} + \tfrac{1}{2}(m(2,0)_{R(L)} - m(2,1)_{R(L)} + m(2,2)_{R(L)} + m(1,5)_{R(L)})]$$

$$\begin{aligned}
\dot{c}_0 &= -\gamma_c c_0 - \frac{\gamma_\parallel}{8\sqrt{\pi}}\left(q(0,0) + \frac{1}{2}\left(q(1,1) + q(2,2)\right)\right) \\
\dot{c}_1 &= -\gamma_c c_1 - \frac{\gamma_\parallel}{16\pi}\left(q(1,1) - q(2,2)\right) \\
\dot{c}_2 &= -\gamma_c c_2 - \frac{\gamma_\parallel}{16\sqrt{\pi}}(q(1,1) + q(2,2))
\end{aligned}$$

$$
\begin{aligned}
\dot{c}_3 &= -\gamma_c c_3 - \frac{\gamma_\parallel}{8\sqrt{2\pi}}(q(0,1)+q(1,0)) \\
\dot{c}_4 &= -\gamma_c c_4 - \frac{\gamma_\parallel}{8\sqrt{2\pi}}(q(0,2)+q(2,0)) \\
\dot{c}_5 &= -\gamma_c c_5 - \frac{\gamma_\parallel}{16\sqrt{\pi}}(q(1,2)+q(2,1)) \\
\dot{d}_{0,R(L)} &= -\gamma_\parallel \left[d_0 - 2\sqrt{\pi} r_0(\tau) + \frac{1}{2\sqrt{\pi}} \left(h(0,0)_{R(L)} + \frac{1}{2}(h(1,1)_{R(L)} + h(2,2)_{R(L)}) \right) \right] \\
\dot{d}_{1,R(L)} &= -\gamma_\parallel \left[d_1 + \frac{1}{4\pi} \left(h(1,1)_{R(L)} - h(2,2)_{R(L)} \right) \right] \\
\dot{d}_{2,R(L)} &= -\gamma_\parallel \left[d_2 - 2\sqrt{\pi} r_2(\tau) + \frac{1}{4\sqrt{\pi}} \left(h(1,1)_{R(L)} + h(2,2)_{R(L)} \right) \right] \\
\dot{d}_{3,R(L)} &= -\gamma_\parallel \left[d_3 + \frac{1}{2\sqrt{2\pi}} \left(h(0,1)_{R(L)} + h(1,0)_{R(L)} \right) \right] \\
\dot{d}_{4,R(L)} &= -\gamma_\parallel \left[d_4 + \frac{1}{2\sqrt{2\pi}} \left(h(0,2)_{R(L)} + h(2,0)_{R(L)} \right) \right] \\
\dot{d}_{5,R(L)} &= -\gamma_\parallel \left[d_5 + \frac{1}{4\sqrt{\pi}} \left(h(1,2)_{R(L)} + h(2,1)_{R(L)} \right) \right]
\end{aligned}
$$

where for the sake of clearness the dependencies in τ have been omitted, and we have defined the auxiliary variables:

$$m(i,j)_{R(L)} = e_{i,R(L)} d_j + e_{i,L(R)} c_j^{(*)} \tag{8}$$

$$q(i,j) = e_{i,R} p^*_{j,L} + e^*_{i,L} p_{j,L} + e_{j,R} p^*_{i,L} + e^*_{j,L} p_{i,R} \tag{9}$$

$$h(i,j)_{R(L)} = e_{i,R(L)} p^*_{j,R(L)} + e^*_{i,R(L)} p_{j,R(L)} + \frac{1}{2}(e_{i,L(R)} p^*_{j,L(R)} + e^*_{i,L(R)} p_{j,L(R)}) \tag{10}$$

References

[1] N. B. Abraham, M. D. Matlin and R. S. Gioggia. Phys. Rev. A **53**, 3514 (1996).

[2] M. Sargent and W. E. Lamb. Phys. Rev **164**, 436 (1967).

[3] D. S. Bakaev, V. M. Ermachenko, V. Yu Kurochin, V. N. Petrovshil, E. D. Protsenko, A. N. Rurukin and Shananin. Sov. J. Quantum. Electron **18**, 1 (1988).

[4] G. C. Puccioni, M. V. Trantnik, J.E. Sipe and G. L. Oppo Opt. Lett. **12**,(1987).

[5] N. B. Abraham, E. Arimondo, M. San Miguel. Optics Comm. **117**, 344 (1995).

[6] For a review see: G. M. Stephan and A. D. May. Quantum Semiclass. Opt. **10**, 19 (1998).

[7] Yu. V. Loiko, A. M. Kulminskii and A. P. Voitovich. Optics. Comm. 210, 121 (2000).

[8] M. D. Matlin, R. S. Gioggia, N. B. Abraham, P. Glorieux and T. Crawford Opt. Comm. **120**, 204 (1995).

[9] J. Redondo, G. J. de Varcárcel and E. Roldán. Phys. Rev. A **56**, 648 (1997).

[10] A. Kulminskii, R. Vilaseca, R. Corbalan and N. B. Abraham, Phys. Rev. A **62**, 648 (2000).

[11] G. C. Puccioni, G. L. Lippi and N. B. Abraham. Optics Comm. **72**, 361 (1989).

[12] C. Taggiasco, R. Meucci, M. Ciofini and N. B. Abraham. Optics Comm. **133**, 507 (1997).

[13] A. Labate, R. Meucci, M. Ciofini, N. B. Abraham and C. Taggiasco. Quantum Semiclass. Opt. **10**, 115 (1998).

[14] I. Leyva, E. Allaria and R. Meucci. Optics Lett. **26**, 605 (2001).

[15] I. Leyva, E. Allaria and R. Meucci. Optics Comm., **217**, 335 (2003).

[16] See, for instance: M. San Miguel, Q. Feng and J. V. Moloney, Phys. Rev. A **52**, 1728 (1995); O. Hess and T. Kuhn. Phys. Rev. A **54**, 3347 (1996); G. Giacomelli, F. Marin and I. Rabbiosi Phys. Rev. Lett. **82**, 675 (1999); or more recently G. D. VanWiggeren and Rajarshi Roy Phys. Rev. Lett. **88**, 097903 (2002).

[17] F. Papoff, G. D'Alessandro and G. L. Oppo. Phys. Rev. A **60**, 648 (1999).

[18] I. Leyva, E. Allaria and R. Meucci. Phys. Rev. A, *in press*.

[19] M. A. van Eijkelenborg, C. A. Schrama and J. P. Woerdman. Optics Comm. **119**, 97 (1995).

[20] A. E. Siegman. *Lasers*. Oxford University Press, Walton Street, Oxford.

[21] Chr. Tamm, Phys. Rev. A **38**, 38 (1988).

[22] A. Labate, R. Meucci and M. Ciofini Optics Comm. **141**, 150 (1997).

[23] *Principles of Optics*. M. Born and E. Wolf. 6^{th} edition. Cambridge University Press (1980).

[24] Chr. Tamm and C. O. Weiss , J. Opt. Soc. Am. B **7**, 1034 (1990).

[25] K. Staliunas, M. F. J. Tarroja and C. O. Weiss. Opt. Comm.**102** 69 (1993).

[26] F. Encinas-Sanz, Oscar G. Calderón, R. Gutiérrez-Castrejón, J.M. Guerra. Phys. Rev. A **59**, 1 (1999).

[27] F. Prati, M Brambilla and L. A. Lugiato. Riv. Nov. Cim. **17**, 1(1994).